Journal of Sound and Vibration (2001) **243**(1), 157–171
doi:10.1006/jsvi.2000.3414, available online at http://www.idealibrary.com on IDEAL®

DESIGN AND SENSITIVITY ANALYSIS OF AN INPUT SHAPING FILTER IN THE *Z*-PLANE

U.-H. Park, J.-W. Lee, B.-D. Lim and Y.-G. Sung

School of Mechanical Engineering, Yeungnam University, 214-1 *Dae-dong Kyungsan*, (*Gyongsan Gyungpuk*) 712-749 *Korea*

(*Received* 13 *April* 2000, *and in final form* 26 *November* 2000)

A variety of input shaper has been proposed to reduce the residual vibration of flexible structures. However, the complexity to solve the non-linear simultaneous equations increases due to addition of the constraints to improve the robustness of an input shaper. In this paper, by proposing a graphical approach which places the shaper zeros on the *z*-plane, the input shaper could conveniently be designed even if the constraints are added for further robustness. Furthermore, it is shown that the proposed method could be accommodated with the variations of both natural frequency and damping ratio. With a mass–damper–spring model, a better performance is obtained using the proposed new multi-hump input shaper.

1. INTRODUCTION

It is necessary to reduce the residual vibration of a light and flexible system for point-to-point operations such as motions of flexible manipulators, ceiling cranes, etc. For vibration reduction, either a feedback or an open-loop control approach could be employed. Instead of using a feedback control, it is possible to eliminate residual vibration with only an open-loop approach. One of the open-loop approaches is the input-shaping technique that employs the convolution of the input shaper with the reference command for vibration reduction.

Smith [1] introduced the posicast control as an input shaper. Recently, Singer and Seering [2, 3] suggested a design method to increase the robustness of Smith's method, using the multiple impulses. Magnitudes and time intervals are obtained by the differentiation of the residual vibration magnitudes with respect to frequency. Singhose, Seering and Singer [4–6] proposed a modified input-shaping technique introducing a multi-hump Extra Insensitive (EI) shaper for robustness improvement. Unfortunately, the calculations are complicated because simultaneous non-linear equations are involved. For damped systems, no analytic solution has been found, so that the solution is numerically presented [7, 8]. Murphy [9] derived an arbitrary rate digital shaping filter from an input-shaping technique. Tuttle and Seering [10] proposed a design method in discrete time domain to cancel out the poles of the systems natural frequencies by the zeros of the input-shaper. They showed that the robustness is improved by adding shaper zeros to the system poles. The shaper provides the smallest time interval with the positive impulse magnitudes. However, their approach should solve the more complicated non-linear simultaneous equations to improve the robustness of the input shaper with the additional constraints. The reason why the difficulty increases is that the sensitivity function of the input shaper is analyzed continuously even if the input shaper is discretely employed.

0022-460X/01/210157 + 15 $35.00/0

In this paper, a method to design the input shaper on the z-plane is proposed by considering the sensitivity function in the discrete time domain. A design procedure of input shapers in both continuous and discrete time domains is reviewed in the next section. The sensitivity equation of the input shaper in the discrete time domain is derived in section 3. In section 4, a brief review of the multi-hump input shaper is given and a method to design a multi-hump input shaper in the discrete time domain is presented. It will be shown that the proposed method has better performance than the existing multi-hump shaper by accounting for the variations of natural frequency and damping ratio simultaneously. In section 5, the performances of multi-hump input shapers in discrete time domain are illustrated.

2. INPUT SHAPER

2.1. CONTINUOUS TIME DOMAIN

At first, the input-shaping technique is briefly reviewed. As an illustration, the input-shaping technique is convolving impulse train with the reference input to eliminate residual vibration. In Figure 1, the responses are shown if a mass–damper–spring system is discretely excited with impulse magnitudes A_0 and A_1. As shown in Figure 1, the first impulse excites the system and then the residual vibration is cancelled out if the second impulse with a damped magnitude A_1 is applied appropriately after half the period of time. In the design of the input shaper, the natural frequency and damping ratio of a system are important factors.

The input shaper is determined from a set of constraint equations that limit the residual vibration of the system. The constraints on vibration amplitude can be expressed as the ratio of residual vibration amplitude with shaping to that without shaping. The ratio [2, 7, 8] is expressed as

$$V(\omega, \zeta) = \mathrm{e}^{-\zeta\omega t_n} \sqrt{\left\{ \sum_{i=0}^{n} A_i \mathrm{e}^{\zeta\omega t_i} \sin(\omega t_i \sqrt{1-\zeta^2}) \right\}^2 + \left\{ \sum_{i=0}^{n} A_i \mathrm{e}^{\zeta\omega t_i} \cos(\omega t_i \sqrt{1-\zeta^2}) \right\}^2}, \tag{1}$$

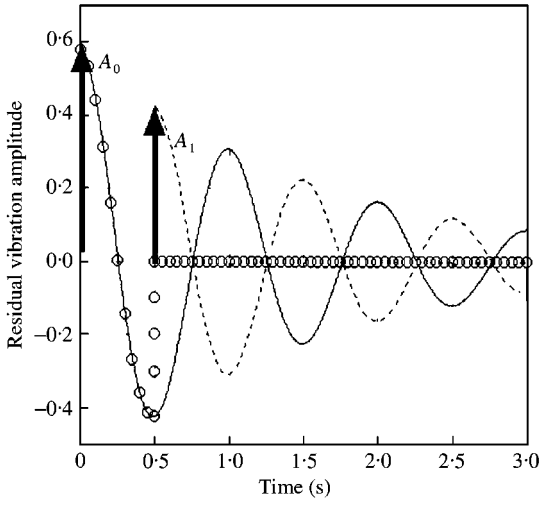

Figure 1. Vibration cancellation using two impulses. ——, Response to A0; - - -, Response to A1; and ○, Response to A0 & A1.

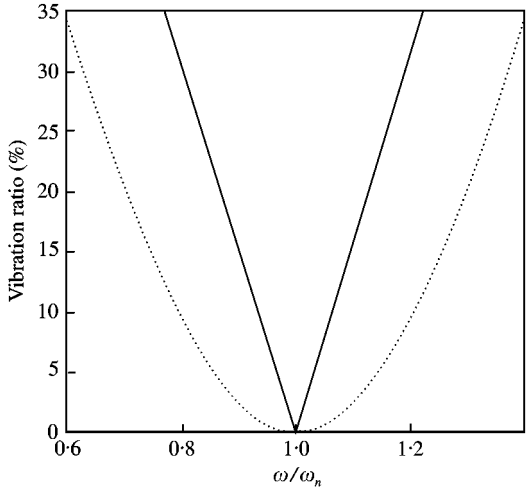

Figure 2. Sensitivity curves for the ZV and ZVD input shapers. ——, ZV shaper; and - - -, ZVD shaper.

where n is one less than the number of impulses, A_i is the amplitude of the ith impulse, t_i is the input time of the ith impulse and t_n is input time of the last impulse. The amplitude and input time can be obtained by using equation (1). The input shaper which reduces the residual vibration by using only two impulses is called a zero-vibration (ZV) input shaper [7, 8]. As shown in Figure 2, the sensitivity curve of the ZV input shaper is shown, with a residual vibration of zero at the point of natural frequency and non-zero in the other frequency region. For reducing the fast growing residual vibration magnitude, a zero-vibration-derivative (ZVD) input shaper [7, 8] is designed by adding the differentiated equations of equation (1). As shown in Figure 2, residual vibration with respect to frequencies is decreased proportionally with the improved robustness.

2.2. DISCRETE TIME DOMAIN

Secondly, the design approach of the input shaper in the discrete time domain is explained with a different aspect from Murphy [9]. The discrete transfer function of the second order system is expressed as

$$G(z) = \frac{1}{(1 - p_1 z^{-1})(1 - p_1^* z^{-1})}, \tag{2}$$

$$\text{where } p_1, p_1^* = \text{Re}^{\pm j\theta}, \quad R = e^{-\zeta\omega_n T}, \quad \theta = \omega_n\sqrt{1-\zeta^2}\,T = \omega_d T.$$

The design strategy of the input shaper cancels out the poles of the system by the zeros of the input shaper which is expressed as

$$H(z) = \tfrac{1}{k}(1 - p_1 z^{-1})(1 - p_1^* z^{-1}) = \tfrac{1}{k}[1 - (p_1 + p_1^*)z^{-1} + p_1 p_1^* z^{-2}], \tag{3}$$

where K is the sum of the coefficients of z^{-n} $(n = 0, 1, 2)$ which normalizes the input shaper.

The poles can be relocated by the impulse time interval T. For example, if the impulse time interval is set to 1/4 of the vibrational period of time, the pole of an undamped system is located on the image axis as shown in Figure 3. The pole moves to the right when T is less

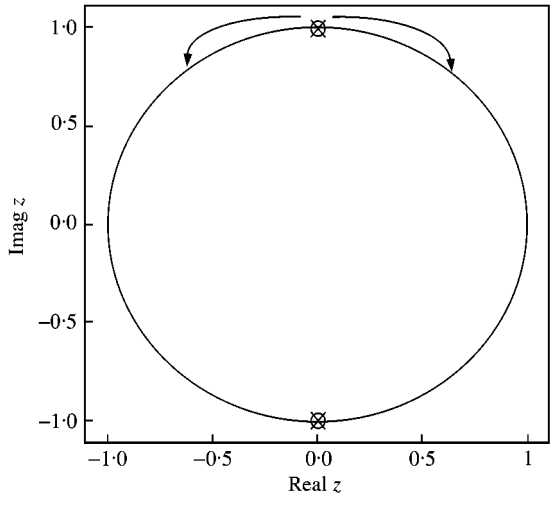

Figure 3. The poles of the system and the zeros of an input shaper in the z-plane.

than 1/4 of the vibrational period of time, and to the left otherwise. If the pole is located in the right half plane, the coefficient of z^{-1} in equation (3) always has a negative sign, so that the system is usually saturated due to the sign change. It is not advisable that the pole be located at the left half plane, which always has the positive coefficient for z^{-1}, since the impulse time interval becomes large. Therefore, the impulse time interval $T = 1/4$ is the optimal time when all the coefficients are positive and the time interval is the smallest. Since $(p + p^*)$ is equal to zero with the impulse time interval $T = 1/4$, equation (3) arrives at equation (4). If $T = 1/2$, the order of input shaper is reduced to one so that equation (4) is expressed as equation (5) which is exactly the same as that of the ZV shaper:

$$H(z) = \tfrac{1}{k}(1 + p_1 p_1^* z^{-2}), \tag{4}$$

$$H(z) = \tfrac{1}{k}(1 - pz^{-1}), \quad K = 1 - p, \quad p = p_1 p_1^*. \tag{5}$$

For increased robustness, extra zeros are added. As a result, the general equation of a ZVD^{n-1} shaper is

$$H(z) = \tfrac{1}{k}(1 - pz^{-1})^n. \tag{6}$$

3. SENSITIVITY CURVE

The sensitivity curve in the discrete time domain is developed by using the input shaper. The sensitivity curve shows how much the amplitude of the residual vibration changes with respect to the frequency. In other words, it is expressed as the ratio between the amplitude of the residual vibration when the input shaper is not used and that of the residual vibration when the input shaper is used. In the continuous time domain, it is equal to V of equation (1). However, in the discrete time domain, V is expressed as

$$V = \frac{|H(z)z^n||G(z)|}{|G(z)|} = |H(z)z^n|. \tag{7}$$

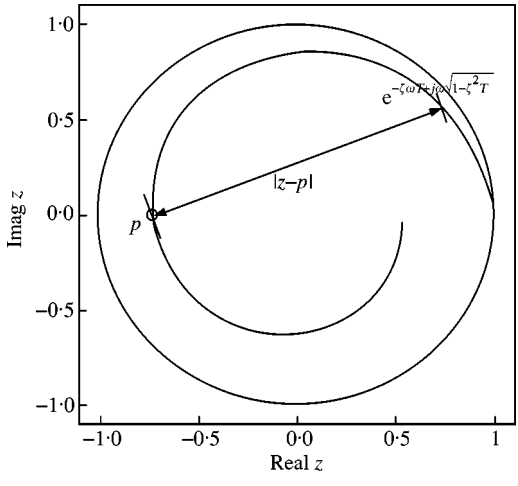

Figure 4. Calculation of $|(1 - pz^{-1})z|$ for ZV input shaper in the z-plane ($T = \pi/\omega_d$).

For mathematical convenience, z^n is multiplied to $H(z)$ for the magnitude comparison of residual vibration between shaped and unshaped inputs. In Appendix A $|H(z)z^n|$ is verified to be the same as V in the continuous time domain.

In the undamped case, the magnitude of $|H(z)z^n|$ is obtained using the graphical method. It is equal to the distance from the zeros of the input shaper to one point on the unit circle $e^{j\omega T}$ divided by K. As shown in Figure 2, the sensitivity curve becomes symmetric with respect to the natural frequency of the system.

In the damped case, $|H(z)z^n|$ is equal to the distance from the zeros of the input shaper to a point on the spiral curve $e^{-\zeta\omega T + j\omega\sqrt{1-\zeta^2 T}}$ divided by K in Figure 4. The sensitivity curve is not symmetric with respect to the natural frequency.

The various types of sensitivity curves could be graphically represented in the discrete time domain.

4. MULTI-HUMP INPUT SHAPER

First, the multi-hump input shaper in the continuous time domain is reviewed for comparison. A design procedure of the multi-hump input shaper is, then, proposed on discrete time domain.

4.1. CONTINUOUS TIME DOMAIN

The multi-hump input shapers have more robustness than the ZVD^{n-1} input shapers for a given residual vibration ratio. This method allows a small amount of residual vibration near the natural frequency of system. As shown in Figure 5, the sensitivity curve indicates a humped shape. The peak of the hump is an allowable residual vibration ratio.

In the case of one-hump, the input shaper with a residual vibration ratio of 5% is obtained by solving simultaneous equations with the condition that residual vibration ratio is equal to zero at $\omega = \omega_{lo}, \omega_{hi}$ and 0.05 at $\omega = \omega_n$. ω_{lo} and ω_{hi} are the lower and upper frequencies where the zero residual vibration occurs. For designing a one-hump input shaper, eight equations are solved for impulse magnitudes A_0, A_1 and A_2, impulse times t_0,

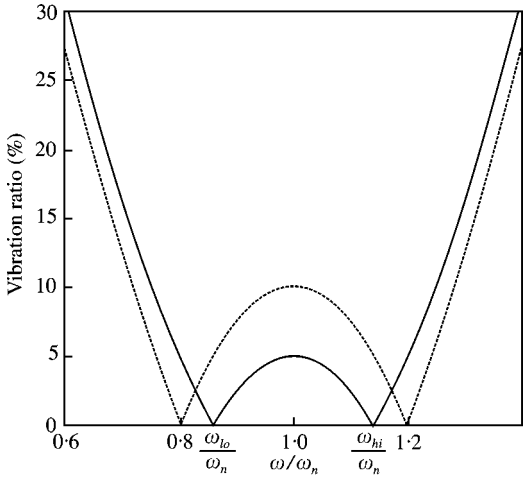

Figure 5. Sensitivity curve of the one-hump input shaper ($V = 5\%$, 10%). ——, $V = 5\%$; and - - -, $V = 10\%$.

t_1 and t_2, and frequencies ω_{lo} and ω_{hi} where the residual vibration becomes 0. For each hump that is added, two more equations are required. Therefore, it is very cumbersome to solve such simultaneous equations. In the case of a damped system, it is more difficult to find an analytic solution. Hence, a numerical solution can be found in reference [8] only for a residual vibration ratio of 5% insensitivity. If the residual vibration ratio for insensitivity is changed, the numerical solution for the coefficient is performed again.

4.2. DISCRETE TIME DOMAIN

A graphical design procedure which places the shaper zeros on the z-plane is described for a multi-hump shaper by considering the variation of natural frequency for the undamped and the damped systems. At the end of the section, the proposed method is extended to the case of the simultaneous variations of natural frequency and damping ratio.

4.2.1. *Design for only frequency variation*

For the undamped system, the zero associated with system pole is located on the unit circle for zero residual vibration with regard to the variation of natural frequency as shown in Figure 6. As in Figure 6(a), if the zeros of input shaper are symmetrically located near the system pole, the system has small residual vibration at the natural frequency (for example $V = 5\%$) and zero residual vibration at the frequency where the input shaper zero is located. If the zeros are placed away from the system pole, the allowance value of the residual vibration increases. Figures 5 and 6(b), respectively, show the sensitivity curve with one hump and zero location in the z-plane with vibration allowance ratio of 10% respectively. In the case of two humps, an input shaper has three zeros. One is located at the system pole and the others are located near the pole as shown in Figure 7. In the case of three humps, the peaks of the two outer hump and the center humps are changed to the normalized locations of ω_{lo1}/ω_n, ω_{lo2}/ω_n ω_{hi1}/ω_n, and ω_{hi2}/ω_n as shown in Figure 8 with $\Delta\omega = \omega_n - \omega_{lo2}$ and $k\Delta\omega = \omega_n - \omega_{lo1}$. The peaks of the three humps can be adjusted by $\Delta\omega/\omega_n$ and $k(0 < k < 1)$. As $\Delta\omega/\omega_n$ increases, so does the height of the outer two humps. The

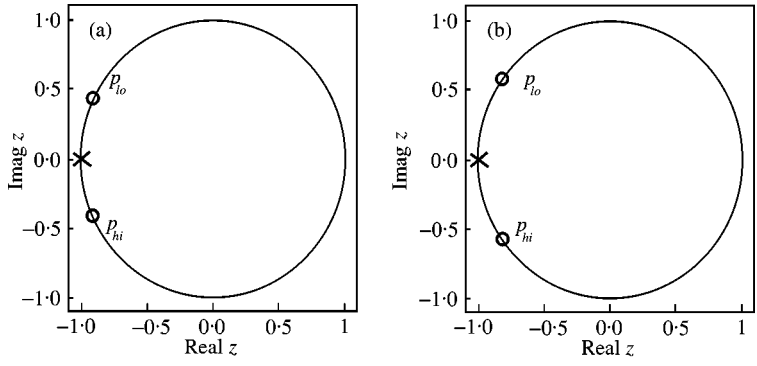

Figure 6. Input shaper zeros with one-hump in the z-plane: (a) $V = 5\%$; (B) $V = 10\%$.

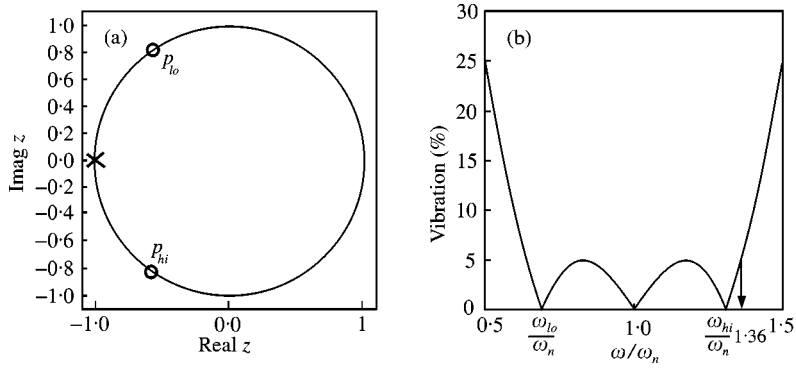

Figure 7. Two-hump input shaper ($V = 5\%$): (a) zeros of a two-hump input shaper; (b) sensitivity curve of a two-hump input shaper.

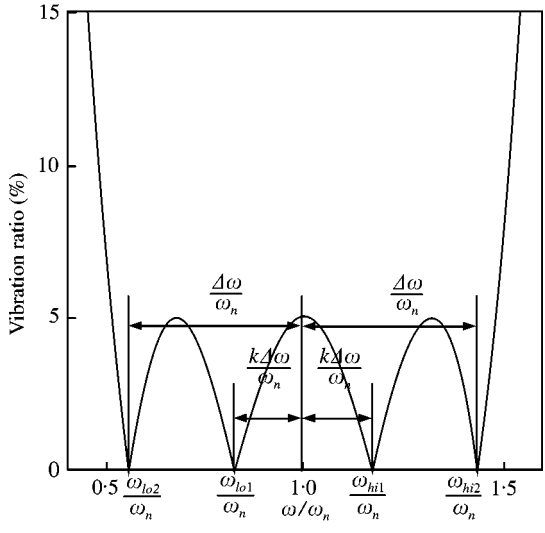

Figure 8. Sensitivity curve of three-hump input shaper.

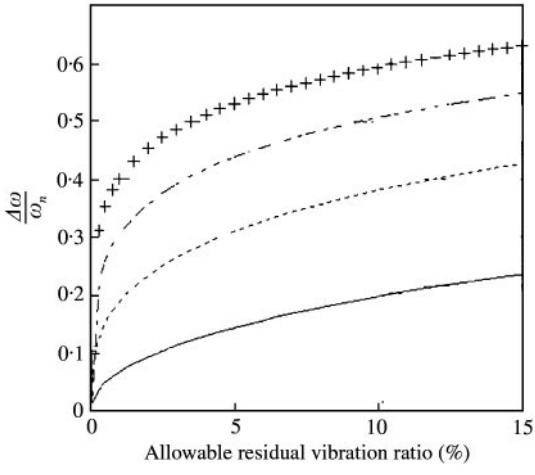

Figure 9. $\Delta\omega/\omega_n$ versus allowable residual vibration for one- and two-hump input shaper. ——, one hump; - - -, two hump; - — - , three hump; + , four hump.

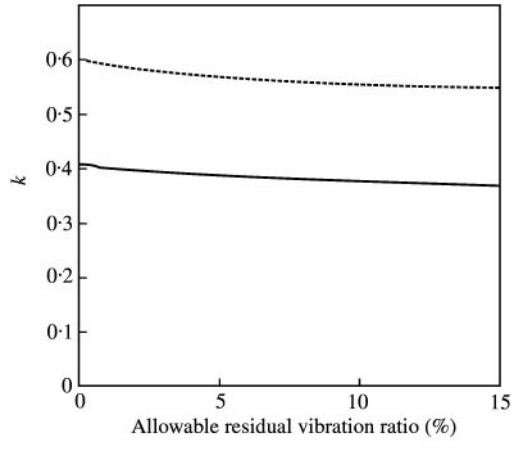

Figure 10. k versus allowable residual vibration for three- and four-hump input shaper. ——, three hump; - - -, four hump.

peak of the center hump increases with increase in the value of k. Figures 9 and 10 show $\Delta\omega/\omega_n$ and k for allowable residual vibration of one-, two-, three- and four-hump input shapers. The zero position of multi-hump input shaper having humps for 5% vibration ratio is shown in Table 1.

In a damped system, the system pole is located on the spiral curve as shown in Figure 11. If the zero positions p_{lo} and p_{hi} are placed on the spiral curve, the coefficient of z^{-n} $(n = 0, 1, 2, \ldots)$ becomes a complex number which is not realizable. However, as shown in Figure 11, if the zeros are located on the circle whose radius is $e^{-\zeta\omega_n T}$, the coefficient of z^{-n} becomes the real number. In the case of a one-hump shaper, there is no frequency at which the residual vibration becomes zero in the sensitivity curve, because no zero is located on the spiral curve, as shown in Figure 11.

In the case of a two-hump shaper, there is a frequency where the residual vibration becomes zero, because one of the zeros is located on the spiral curve. The zero positions of input shapers are shown in Table 1 with a damping ratio of $\zeta = 0{\cdot}1$. Figure 12 shows the

TABLE 1

Zero position of input shaper having uneven sensitivity ($V = 5\%$)

The number of Humps	Zero positions of multi-hump EI shaper	$\zeta = 0$		$\zeta = 0{\cdot}1$	
		$\Delta\omega/\omega_n$	k	$\Delta\omega/\omega_n$	k
1	$p_{hi,lo} = e^{-\zeta\omega_n T + j(1 \pm (\Delta\omega/\omega_n))\pi}$	0·1400		0·1650	
2	$p_{\omega_n} = e^{(-\zeta\omega_n + j\omega_n)T}$ $p_{hi,lo} = e^{-\zeta\omega_n T + j(1 \pm (\Delta\omega/\omega_n))\pi}$	0·3088		0·3500	
3	$p_{hi1,lo1} = e^{-\zeta\omega_n T + j(1 \pm (k\Delta\omega/\omega_n))\pi}$ $p_{hi2,lo2} = e^{-\zeta\omega_n T + j(1 \pm (\Delta\omega/\omega_n))\pi}$	0·4376	0·387	0·4840	0·425
4	$p_{\omega_n} = e^{(-\zeta\omega_n + j\omega_d)T}$ $p_{hi1,lo1} = e^{-\zeta\omega_n T + j(1 \pm (k\Delta\omega/\omega_n))\pi}$ $p_{hi2,lo2} = e^{-\zeta\omega_n T + j(1 \pm (\Delta\omega/\omega_n))\pi}$	0·5306	0·5703	0·5722	0·6154

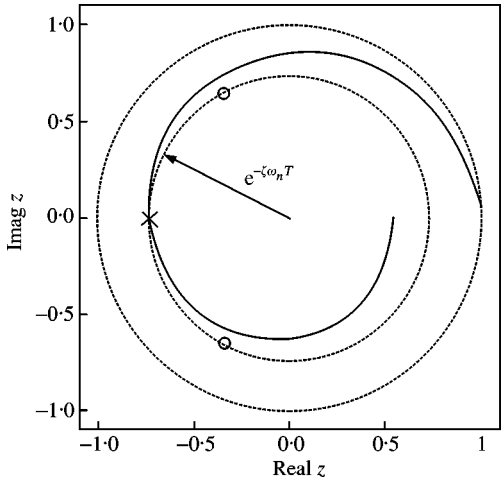

Figure 11. Input shaper zeros with one hump in the z-plane ($V = 5\%$, $\zeta = 0{\cdot}1$, $\omega_n = 4 \times 2\pi$ rad/s).

sensitivity curve of one- and two-hump input shapers. Figures 13 and 14 show $\Delta\omega_n/\omega_n$ and k for allowable residual vibration of one-, two-, three- and four-hump shapers.

As previously illustrated, the input shaper in the discrete time domain is readily obtained because the proposed technique is treated with the least number of variables compared to the one in the continuous time domain. For input shaper designs having one- or two-hump shapers, the z-plane technique uses only $\Delta\omega/\omega_n$. In the case of three- and four-hump shapers, the additional variable k is involved. When the number of humps increases by two, the relevant number of variables increases by one. However, an input shaper having more than five humps is not practical because of a large time delay in actual implementation.

4.2.2. *Design for both frequency and damping ratio variations*

The existing design procedure [4–6] of a multi-hump shaper does not consider the variation of damping ratio as shown in Figure 15. However, a multi-hump shaper could be

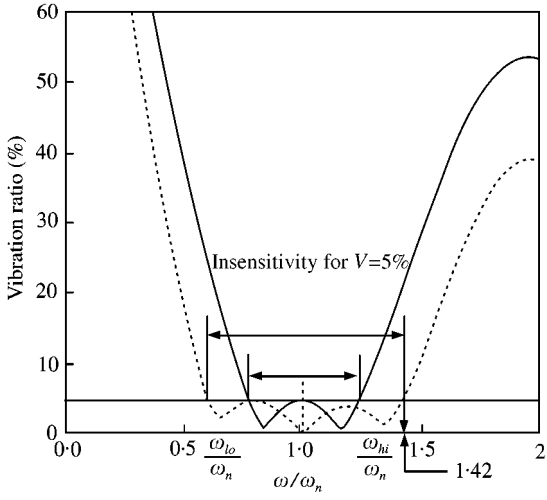

Figure 12. Sensitivity curves of one- and two-hump input shapers ($V = 5\%$, $\zeta = 0{\cdot}1$, $\omega_n = 4 \times 2\pi$ rad/s). ——, one hump; and - - -, two hump.

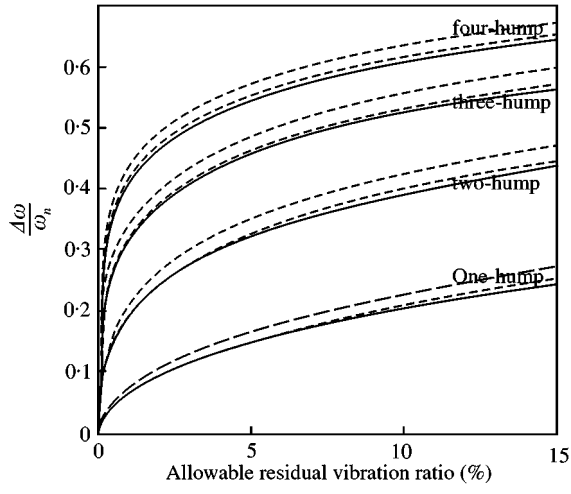

Figure 13. $\Delta\omega/\omega_n$ versus allowable residual vibration for one-, two-, three- and four-hump input shapers. (damped system). ——, damping ratio: 0·03; - - -, damping ratio: 0·05; and - — -, damping ratio: 0·1.

extended to the case of the simultaneous variations of both natural frequency and damping ratio by the proposed graphical method.

For an example, a two-hump shaper with the frequency variation 0–8 Hz is designed when the natural frequency of the system is 4 Hz. In the case of the constant ζ in Figure 11, the behavior of the spiral curve always moves into the inside of the inner circle according to the frequency increment. However, the spiral curve goes to either the inside or the outside of the inner circle in the case of the variations of both damping ratio and frequency as shown in Figure 16. The sensitivity curves of the two-hump shaper on plane ζ and ω/ω_n are shown in Figure 17. The proposed graphical design method could account for the variation of both natural frequency and damping ratio. When the damping ratio varies from 0·28 to 0·02, the proposed method has better performance than Singhose's in Figure 18.

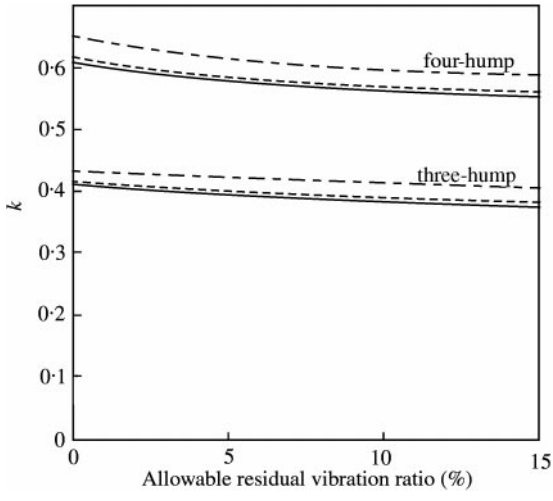

Figure 14. k versus allowable residual vibration ratio for a three-hump input shapers (damped system). ——, damping ratio: 0·03; – – –, damping ratio: 0·05; and - - -, damping ratio: 0·1.

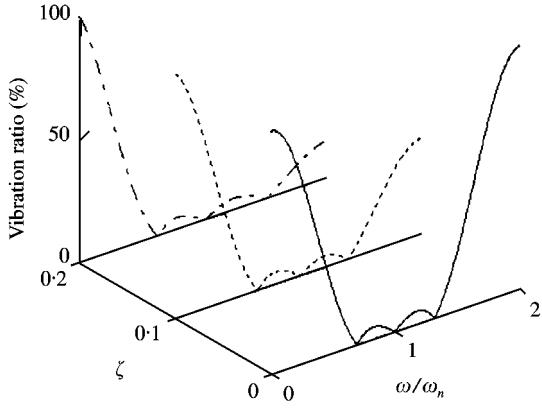

Figure 15. Sensitivity curves of Singhose's two-hump shapers. ——, zeta = 0; – – –, zeta = 0·1; and - - - , zeta = 0·2.

5. SIMULATION

A mass–damper–spring system is employed as shown in Figure 19 to demonstrate the efficacy of the proposed technique.

In the undamped case, the step input is applied to mass 1 where masses m_1 and m_2 are 1 kg and the spring constant k is 632 N/m. Figure 20 shows the impulse sequence of a two-hump shaper for the system. When a two-hump input shaper is used, the residual vibration is shown in Figure 21. By assigning a spring constant of $k = 1168$ N/m, which gives a 36% variation on the natural frequency, the amplitude of the residual vibration is observed to be within 5%, as expected in Figure 7(b).

In the damped case, Figure 22 shows the impulse sequence of a two-hump shaper. Figure 23 shows the numerical result of taking a spring constant of 1274 N/m, which gives a 42% variation in the natural frequency, and a damped coefficient 5·03 N s/m. This gives a 5% variation, as shown in Figure 12. At the last impulse time, the envelope of the damped system hits 5%.

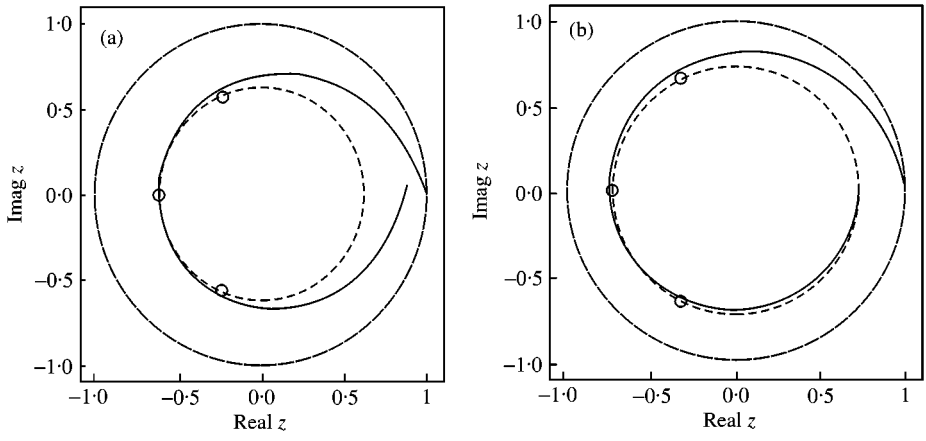

Figure 16. Zeros of two-hump shaper: (a) damping ratio (0·28–0·02); (b) damping ratio (0·1–0·05).

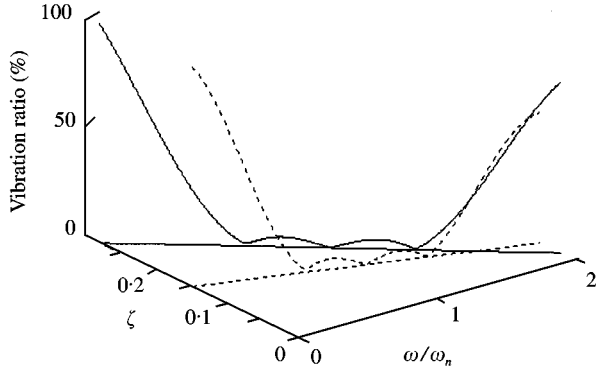

Figure 17. Sensitivity curve of two-hump shaper designed to frequency and damping ratio variations. ——, zeta = 0·28–0·02; and - - -, zeta = 0·15–0·05.

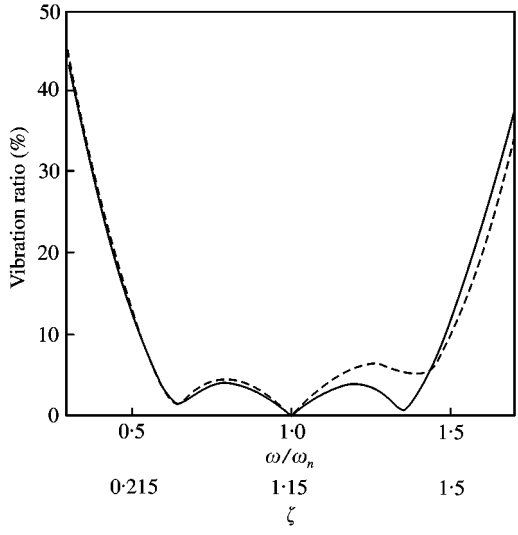

Figure 18. Sensitivity curves of two-hump shapers. ——, Proposed shaper; and - - -, Singhose's shaper.

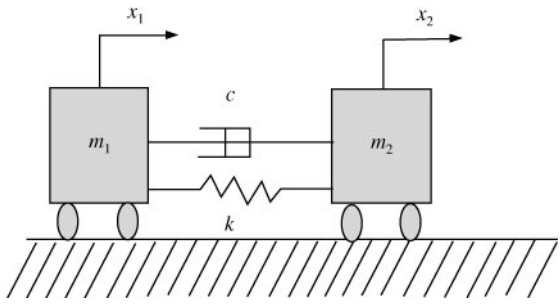

Figure 19. Two mass, spring and damper model.

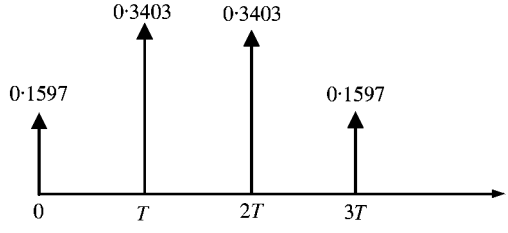

Figure 20. Impulse sequence for two-hump shaper for undamped system ($T = 0{\cdot}125$).

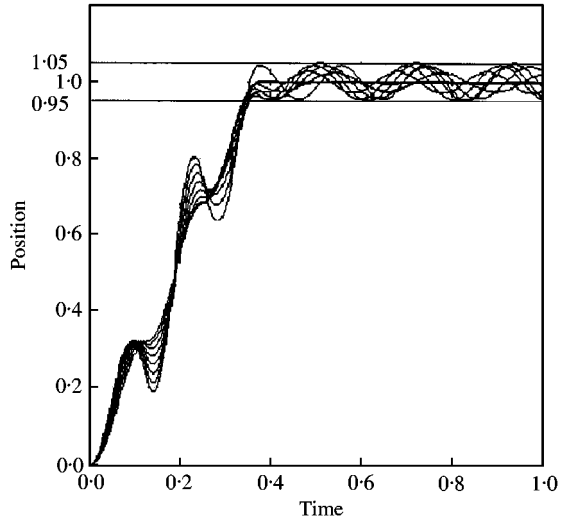

Figure 21. Time response with two-hump shaper for the undamped system.

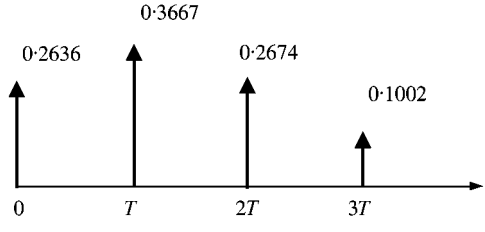

Figure 22. Impulse sequence of two-hump shaper for damped system ($T = 0{\cdot}1256$).

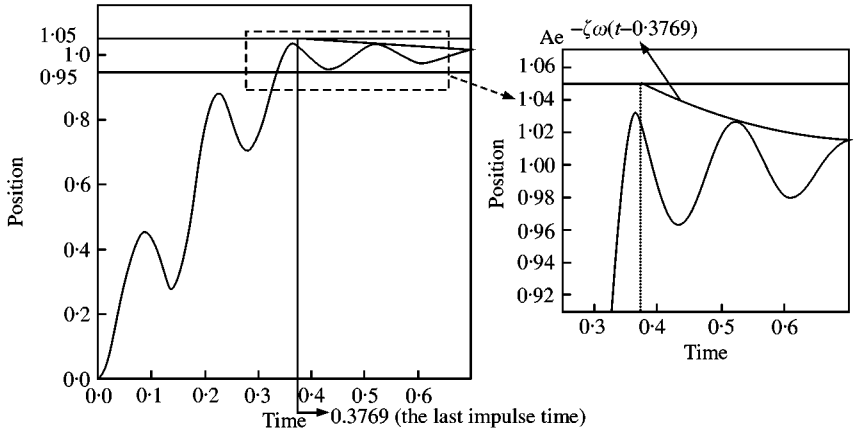

Figure 23. Time response with two-hump shaper for damped system.

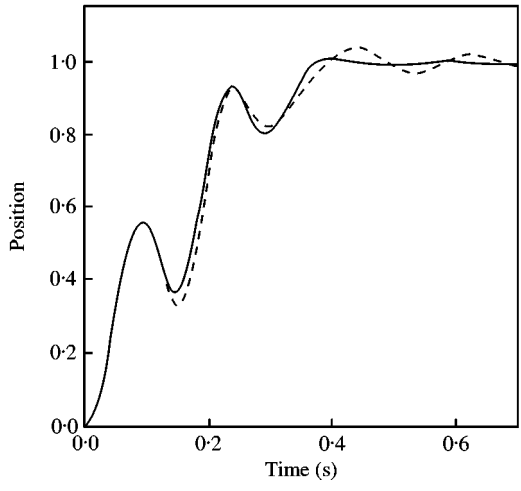

Figure 24. Time response with two-hump shapers for step input. ——, Proposed shaper; and - - -, Singhose's shaper.

For an instance, when the natural frequency of a system of 4 Hz is changed to 5·4 Hz and the damping ratio 0·15 is changed to 0·1, the step input is applied to the mass–damper–spring system with two-hump shaper. As expected in Figure 18, the performance of the proposed method is better than that of Singhose's as shown in Figure 24.

6. CONCLUSION

In this paper, it is shown that the sensitivity function in the z-plane is equal to the one in the continuous time domain. In order to obtain the desired shape of the sensitivity curve, the graphical design method, which adjusts the zeros of input shapers on the z-plane, is presented. The graphical method does not solve non-linear simultaneous equations to design a robust multi-hump shaper. Unlike the existing design method, the proposed method could accommodate with the simultaneous variation of natural frequency and

damping ratio. It was shown that the newly designed shaper has better performance than the existing multi-hump shaper. With a mass–damper–spring model, the performance of the proposed multi-hump shaper was illustrated.

ACKNOWLEDGMENT

The research described in this paper was supported through the Regional Research Center (RRC) of Yeungnam University.

REFERENCES

1. T. SMITH 1958 *IRE Transactions on Automatic Control* **AC-3**, 14–23. Analog study of dead-beat posicast control.
2. N. C. SINGER and W. P. SEERING 1989 *Proceedings of American Control Conference* 1738–1744. Experimental verification of command shaping method for controlling residual vibration in flexible robot.
3. N. C. SINGER and W. P. SEERING 1990 *Journal of Dynamic System, Measurement and Control* **112**, 76–82. Preshaping command input to reduce system vibration.
4. N. C. SINGER and W. P. SEERING 1992 *International Conference on Robotics and Automation* 800–805. An extension of command shaping methods for controlling residual vibration using frequency sampling.
5. W. E. SINGHOSE and N. C. SINGER 1994 *IEEE Conference On Control Applications*, Glasgow, Scotland. Input shapers for improving the throughput of torque-limited systems.
6. W. E. SINGHOSE, W. P. SEERING and N. C. SINGER 1994 *Journal Mechanical Design* **116**. Residual vibration reduction using vector diagrams to generate shaped inputs.
7. W. E. SINGHOSE, L. J. PROTER, T. D. TUTTLE and N. C. SINGER 1997 *Journal of dynamic systems, Measurement, and control* **199**, 320–326. Vibration reduction using multi-hump input shapers.
8. W. E. SINGHOSE, W. P. SEERING and N. C. SINGER 1997 *Journal of Dynamic System, Measurement, and Control* **119**, 198–205. Time-optimal negative input shapers.
9. B. R. MURPHY and ICHIRO WATANBE 1992 *IEEE Transaction on Robotics and Automation* **8**, 285–289. Digital shapers for reducing machine vibration.
10. T. D. TUTTLE and W. P. SEERING 1994 *American Control Conference* 2533–2537. A zero-placement technique for designing shaped inputs to suppress multiple-mode vibration.

APPENDIX A

$|H(z)z^n|$ is expressed as equation (A) using $s = -\zeta\omega + j\omega\sqrt{1-\zeta^2}$ and $z = e^{sT}$.

$$|H(z)z^n| = |A_0 e^{(-\zeta\omega + j\omega\sqrt{1-\zeta^2})nT} + A_1 e^{(-\zeta\omega + j\omega\sqrt{1-\zeta^2})(n-1)T} + , \ldots , + A_n| \quad \text{(A)}$$

where, nT is equal to t_n of equation (1). Therefore, equation (A) is rewritten as

$$|H(z)z^n| = |A_0 e^{(-\zeta\omega + j\omega\sqrt{1-\zeta^2})t_n} + A_1 e^{(-\zeta\omega + j\omega\sqrt{1-\zeta^2})t_{n-1}} + , \ldots , + A_n| \quad \text{(B)}$$

On the other hand, equation (1) is rewritten as

$$V = |A_0 e^{-\zeta\omega t_n + j\omega\sqrt{1-\zeta^2}t_0} + A_1 e^{-\zeta\omega t_{n-1} + j\omega\sqrt{1-\zeta^2}t_1} + , \ldots , + A_n| \quad \text{(C)}$$

Comparing equations (B) and (C), we can see the equality.